JOURNAL OF SYNCHROTRON RADIATION
ISSN 1600-5775

Multifarious injection chamber for molecular structure study (MICOSS) system: development and application for serial femtosecond crystallography at Pohang Accelerator Laboratory X-ray Free-Electron Laser

Received 29 September 2017
Accepted 4 January 2018

Edited by M. Yabashi, RIKEN SPring-8 Center, Japan

Keywords: serial femtosecond crystallography; PAL-XFEL; lysozyme; NCI; sample injector; MICOSS.

Jaehyun Park,* Seonghan Kim, Sangsoo Kim and Ki Hyun Nam

Pohang Accelerator Laboratory, POSTECH, Pohang, Gyeongbuk 37673, Republic of Korea.
*Correspondence e-mail: fermi13@postech.ac.kr

The multifarious injection chamber for molecular structure study (MICOSS) experimental system has been developed at the Pohang Accelerator Laboratory X-ray Free-Electron Laser for conducting serial femtosecond crystallography. This system comprises several instruments such as a dedicated sample chamber, sample injectors, sample environment diagnostic system and detector stage for convenient distance manipulation. Serial femtosecond crystallography experiments of lysozyme crystals have been conducted successfully. The diffraction peaks have reached to ~1.8 Å resolution at the photon energy of 9.785 keV.

1. Introduction

Data collected at X-ray free-electron laser facilities (Emma *et al.*, 2010; Ishikawa *et al.*, 2012) can reveal the ultrafine structures of macromolecular crystals by using almost fully coherent X-ray beams with very high photon flux and ultrashort pulses (Boutet *et al.*, 2012; Chapman *et al.*, 2011; McNeil & Thompson, 2010). Owing to these features of the light source, detailed information about the molecular structure can be obtained at room temperature before radiation damage occurs (Neutze *et al.*, 2000). However, to obtain three-dimensional data before radiation damage occurs, small crystals need to be delivered serially or *via* measurement on a large crystal that is being translated and rotated between shots in order to avoid radiation damage.

Studies have investigated various methods for delivering samples in a fully hydrated state. Droplet stream generation has been used to deliver crystals that interact with repeated X-ray pulses (Weierstall *et al.*, 2008). A continuous liquid jet injector with a gas dynamic virtual nozzle (GDVN) has been developed to solve the problem of crystal clogging (Weierstall *et al.*, 2012). Electrospinning and lipidic cubic phase (LCP) sample delivery methods have been used to handle the issue of high sample consumption (Sierra *et al.*, 2012; Weierstall *et al.*, 2014). The LCP jet was developed to be able to inject extremely viscous material. That it has lower sample consumption is a benefit to the high-viscosity media that it was designed to inject.

Serial femtosecond crystallography (SFX) experiments have been conducted successfully at the Linac Coherent Light Source (LCLS) (Barends *et al.*, 2014; Boutet *et al.*, 2012; Chapman *et al.*, 2011; Kern *et al.*, 2013; Redecke *et al.*, 2013) and SPring-8 Ångstrom Compact free-electron LAser

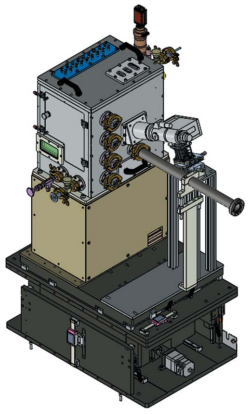

(SACLA) (Sugahara *et al.*, 2015) with existing sample delivery methods. A vacuum chamber affords the advantage of high signal-to-noise (S/N) ratio with low scattering background; however, it has disadvantages such as evaporative cooling of the injected liquid stream and phase transition of the crystal delivery medium. In the case of LCP, a medium with different composition is required to solve the phase-transition problem in vacuum (Liu *et al.*, 2014). A helium-gas-filled sample chamber provides relatively a lower S/N ratio for diffraction data compared with a vacuum chamber, but it helps to overcome the phase-transition problem of an LCP carrier (Tono *et al.*, 2015).

Recently, the Pohang Accelerator Laboratory X-ray Free-Electron Laser (PAL-XFEL) has been commissioned and operated for delivering X-ray laser pulses using a 10 GeV linear accelerator (Ko *et al.*, 2017). We have developed an experimental system for SFX with microfocused X-ray pulses at the Nano Crystallography and Coherent Imaging (NCI) experimental station at PAL-XFEL (Park *et al.*, 2016). This system is called the multifarious injection chamber for molecular structure study (MICOSS). It provides efficient operational performance for SFX at PAL-XFEL. In this study, we describe its design and performance. In particular, we have applied a gas-filling concept to the sample chamber operation at ambient pressure to focus on the delivery of a highly viscous matrix and to avoid phase transition of the carrier. By using this system, clear diffraction patterns have been obtained for lysozyme microcrystals.

2. MICOSS system design

The MICOSS system has been designed to conduct SFX experiments efficiently. It comprises sample injectors, a dedicated chamber and a detector manipulation system.

2.1. Sample injector

The sample injector used for delivering samples is a very important factor in SFX experiments in light of the radiation damage caused to crystals when they are illuminated by XFEL pulses with exceedingly high photon flux. Two types of sample injectors have been widely used thus far. A GDVN-based liquid jet injector generates a thin continuous liquid stream (Deponte, Mckeown *et al.*, 2011; DePonte, Nass *et al.*, 2011; Weierstall *et al.*, 2012). An LCP sample injector is used for delivering highly viscous crystal-mixed matrix carriers such as monoolein (Weierstall *et al.*, 2014), grease matrices (Sugahara *et al.*, 2015) or other high-viscosity matrices (Botha *et al.*, 2015).

2.1.1. Operational injectors. We have developed two types of sample injector systems: (i) Particle Solution Delivery (PSD) injectors for the delivery of crystals or particles in solution and (ii) Carrier Matrix Delivery (CMD) injectors for the delivery of crystals grown or embedded in LCP and other highly viscous carriers.

The PSD injector nozzle consists of a glass capillary for gas focusing and a tapered capillary for delivering the sample suspension. The outer diameter of the tapered capillary is 360 µm, and typical inner diameters are 50, 75, 100, 150 and 200 µm. If particle clogging occurs, only tapered capillaries can be replaced in the nozzle structure. The gas-focusing capillary, with inner diameter of ∼900 µm, surrounds the tapered capillary with coaxial geometry. Both fluidic channels meet together with a Tee fitting (Fig. 1*a*). The glass capillary is directly attached to the Tee fitting; the tapered capillary passes through the Tee fitting and is located inside the glass capillary. A helium gas stream is provided through the other port of the Tee fitting. The sample nozzle and external sample input channel are connected through custom-made double male nuts of 10–32 pitch; these are advantageous because they shorten the fluidic delivery length.

The CMD injector uses a piston to deliver samples with high pressure and low flow rate (Fig. 1*c*). The sample in the reservoir is extruded by a nozzle unit having a structure similar to that of the PSD injector. The helium gas flow with coaxial geometry in the nozzle guides the extruded sample along a straight path. The volume of the sample reservoir is 40 µl; it is operated continuously for 5 h with a flow rate of ∼130 nl min^{-1}. The extruding diameter is varied as 75, 100 and 150 µm depending on the crystal size. The CMD injector is

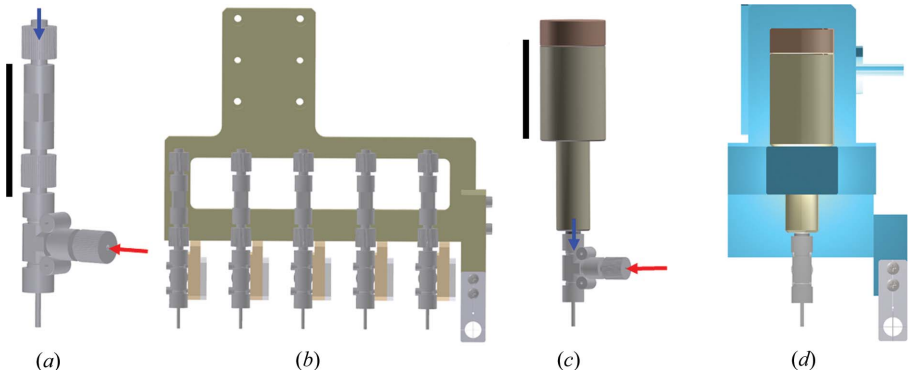

Figure 1
(*a*) PSD injector nozzle. (*b*) Multi PSD nozzle system. (*c*) CMD injector. (*d*) CMD injector holding geometry. Blue and red arrows indicate the input ports for liquid sample and helium gas, respectively. The black scale bars represent 30 mm.

installed inside MICOSS with a compact holder, as shown in Fig. 1(*d*).

2.1.2. Multinozzle system. The stable operation of GDVN-based sample injectors is strongly influenced by the size of the crystals inserted into the fluidic path of the injector nozzle. An unexpectedly large cluster of particles or crystals can clog the injection system. To prevent complete injector nozzle exchange, which is time consuming, a multinozzle injector system is used to achieve higher efficiency. As shown in Fig. 1(*b*), five injector nozzles can be installed simultaneously. When a liquid jet nozzle is clogged, a fresh nozzle can be used for the operation immediately by changing the fluidic channel in the valve system. In addition, a kinetic mount scheme is applied to the injector nozzle installation by using magnets for fast and convenient exchange.

2.2. MICOSS

MICOSS has been designed to operate various sample injectors, and it incorporates X-ray focusing optics and diagnostic tools. Fig. 2 shows the design of the chamber system. The chamber has dimensions of 400 × 430 × 300 mm. The chamber position is manipulated by two-dimensional motorized stages whose directions are perpendicular to the incident optical path of XFEL pulses. It includes various instruments for X-ray and liquid beam diagnosis and injector manipulation in the controlled sample environments.

2.2.1. Optics alignment and diagnostics. K-B mirror optics has been installed to focus XFEL pulses to a spot size of ∼2 µm at the sample position. The focal length between the sample and the center of the mirror chamber is ∼5.68 m (Park *et al.*, 2016). A pinhole aperture is installed on a pinhole holder that is manipulated by two-dimensional piezo stages inside the chamber to block the scattering background from spontaneous radiation (Fig. 3*a*). The horizontally and vertically focused beam size is measured by the knife-edge scanning method. A holder for tungsten or gold wires (diameter: 200 µm) in the cross geometry is attached to the injector holding structure, as shown in Fig. 3(*b*). The scanning beam intensity is measured using a photodiode (PD) located ∼4 m downstream from the sample position during the K-B mirror alignment process. However, during the SFX experiment, because the beam is blocked by the large-area CCD detector, the PD at the downstream location cannot be used simultaneously. To monitor the beam intensity and measure the focused beamsize immediately, a PD is installed near the rear wall of the chamber but during the beam measurements the beam intensity must be reduced using a solid attenuator. The PD is attached to a 90° rotatable arm to enable it to approach the center of the large-area window of the detector with minimum spatial consumption, as shown in Fig. 3(*c*).

The environment near the sample position strongly influences the sample stability and diffraction signal quality. At the bottom of the chamber side wall, sensors are placed to detect the environmental conditions, as shown in Fig. 3(*d*). An oxygen concentration sensor is used to check the filling status of helium gas inside the chamber; a temperature and humidity sensor is also installed.

2.2.2. Sample catcher. High-speed liquid beam injection by a PSD injector nozzle can evaporate the samples and contaminate the inside of the chamber. A sample catcher is installed just below the PSD injector nozzle end, as shown in Fig. 3(*e*). The entrance hole for the incident X-ray pulses is about 4.5 mm in diameter as shown in Fig. 3(*f*). The nozzle end, near the XFEL beam interaction point, is located at the elliptical hole (which covers ±48° solid angle for diffracted X-rays) center.

2.2.3. X-ray beam ports and stopper. The window port for passing scattered X-ray signals to the detector is located downstream of the chamber. The detector port is wrapped

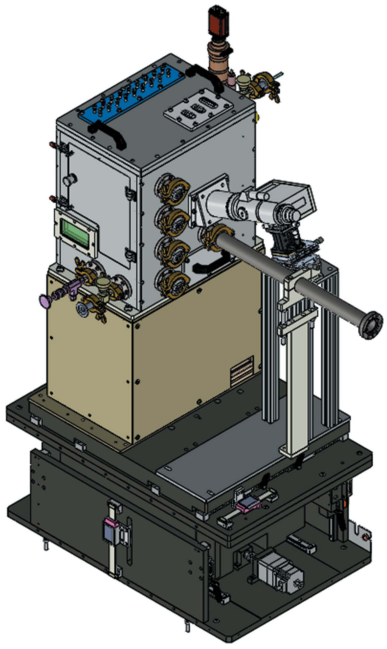

Figure 2
MICOSS and position manipulation stage.

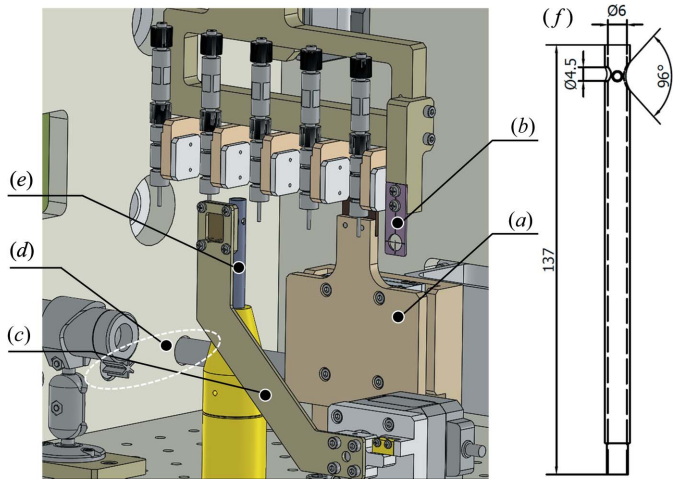

Figure 3
(*a*) Pinhole position (two-dimensional) manipulator. (*b*) Cross wire holder. (*c*) PD position manipulator. (*d*) Chamber environment sensors for oxygen concentration and humidity. (*e*) Sample catcher. (*f*) Drawing of the sample catcher rod. The length unit is mm.

with a polyimide film (thickness: 125 µm, films of different thicknesses are available if required; diameter: 203 mm); it covers the diffraction angle of ±48° (Fig. 4*a*). A cylindrical direct X-ray beam stopper (diameter: 3 mm) is installed just in front of the window. An aluminium cylinder (diameter: 2 mm; height: 7 mm) is inserted into the tungsten holder (length: 15 mm). The holder body is connected with a plate attached vertically near the top of the detector port.

Incident XFEL pulses are introduced through an NW40 Kwik-Flange, as shown in Fig. 4(*d*). The beam transport pipe is connected to the beamline end that is blocked by a beryllium window (thickness: 60 µm; diameter: 10 mm). The inside of the pipe is filled with helium gas during the experiments.

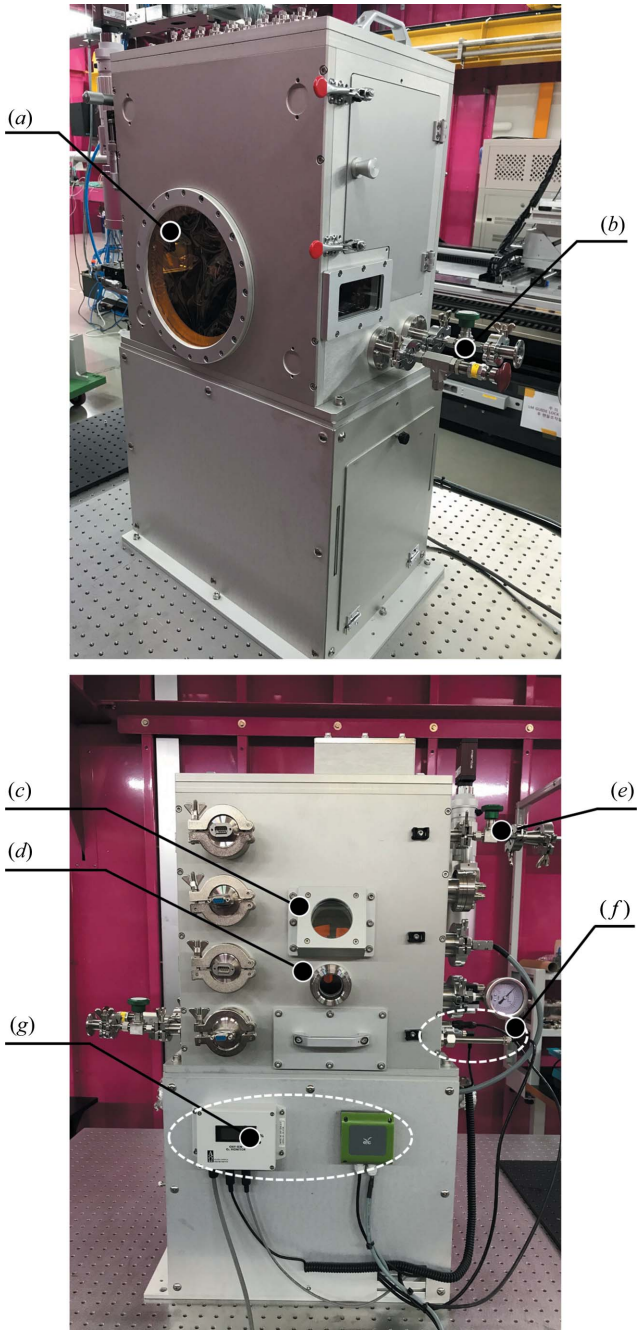

Figure 4
(*a*) Window for passing diffraction signal to detector. (*b*) Pumping port. (*c*) View port for microscope. (*d*) XFEL pulse input port. (*e*) Helium gas input port. (*f*) Sensors (oxygen and humidity). (*g*) Sensor controllers.

2.2.4. Injector manipulation. The sample flow is controlled by a high-performance liquid chromatography (HPLC) pump system (LC-20AD, Shimadzu) with double six-channel, seven-port switching valves. The pump can be operated from the NCI hutch control room by using a remote-control module (CBM-20 A, Shimadzu).

The nozzle position is manipulated by using a combination of three high-precision linear motion stages with typical resolution of 50 nm. The travel range is 200, 100 and 50 mm along the horizontal, vertical and XFEL beam directions, respectively. The horizontal travel range covers the entire necessary range of the multiport nozzle operation. This stage system can also be used to manipulate the cross wire holder. The stage resolution is sufficient to accurately measure a focused X-ray beam size of ∼2 µm.

2.2.5. Sample injector monitoring. The injection operation status strongly depends on the crystal clustering and delivery medium conditions. It is important to monitor the injection condition to align the extruded sample beam with the XFEL pulses and to conduct experiments efficiently for judging nozzle clogging and sample conditions. Two microscopes with a long-working-distance lens (UWZ300F; working distance: 300 mm) and a CCD camera (G-046, Manta; resolution: 780 × 580 pixels; pixel size: 8.3 µm) are installed around the chamber body. One microscope is installed in front of the chamber to observe the sample in the lateral position through a tilted viewport, as shown in Fig. 4(*c*), and the other is installed so as to observe the sample in the vertical position at the side of MICOSS.

2.3. Detector and manipulation stage

An MX225-HS (Rayonix) is installed downstream of the sample chamber. The sensing area is 225 × 225 mm, and the resolution is 5760 × 5760 pixels. The frame rate depends on the chip binning option; for example, the frame rate for 2 × 2 and 4 × 4 binning modes is 10 and 40 frames s^{-1}, respectively. The available resolution is 1.5 Å at 100 mm distance from the sample with X-ray beam energy of 10 keV.

Here, the sample-to-detector distance must be optimized to maximize the resolution; the peak separation is affected by the reciprocal lattice constants. For efficient and simple adjustment of the distance, a detector stage was designed and developed. The available distance range is 90–4000 mm, and the position can be manipulated in each direction by using the motorized stage.

3. Experiment and results

To evaluate the MICOSS system, we performed SFX experiments at the NCI station. Fig. 5 shows the experimental setup. The incident XFEL beam has a pink spectrum (∼0.3% bandwidth) and a centered photon energy of 9.785 keV (1.27 Å) with ∼5 × 10^{10} photons $pulse^{-1}$ (repetition rate:

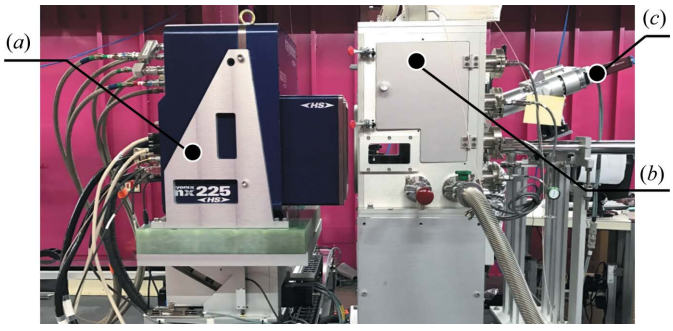

Figure 5
SFX experiment setup. (*a*) MX225-HS (Rayonix). (*b*) MICOSS. (*c*) Sample viewing microscope.

10 Hz). The focused X-ray beam size was 2.5 (H) × 3.0 (V) µm (FWHM). The MX225-HS detector was installed on the detector stage and operated in the 2 × 2 binning mode. The sample-to-detector distance was 90 mm. Lysozyme crystals (30 × 30 × 30 µm), a model sample embedded in monoolein, were delivered using the CMD injector with a 100 µm-diameter nozzle. The focused XFEL pulses intersected the extrusion near the end, as shown in Fig. 6(*a*). The sample flow rate was controlled to ∼130 nl min^{-1} under stable extrusion.

Diffracted images were filtered using the *NanoPeakCell* program based on the threshold algorithm (Coquelle *et al.*, 2015). Fig. 6(*b*) shows a representative diffraction pattern to 1.8 Å resolution collected from the lysozyme crystal sample. The diffraction pattern was indexed using *CrystFEL*, as shown in Fig. 6(*c*) (White *et al.*, 2016). The structure determination is in progress.

4. Conclusion

We have reported the development of an experimental system for SFX at the NCI station at PAL-XFEL. To evaluate the developed instruments, we performed experiments using lysozyme crystals, and we confirmed the successful operation of the system. This system is designed for SFX studies; however, it can be applied to various applications by using the same injector and sample environment. In fact, by using the same system, we could also perform liquidography experiments. The MICOSS system can potentially be used in the fields of not only biology but also chemistry and physics for conducting small- and wide-angle X-ray scattering experiments. In the future, the MICOSS system will be further upgraded for applications to time-resolved studies.

Acknowledgements

We would like to acknowledge all members of the PAL-XFEL. This work was funded by the Ministry of Science, ICT and Future Planning (MSIP), the Republic of Korea, through the PAL-XFEL project.

References

Barends, T. R. M., Foucar, L., Botha, S., Doak, R. B., Shoeman, R. L., Nass, K., Koglin, J. E., Williams, G. J., Boutet, S., Messerschmidt, M. & Schlichting, I. (2014). *Nature (London)*, **505**, 244–247.
Botha, S., Nass, K., Barends, T. R. M., Kabsch, W., Latz, B., Dworkowski, F., Foucar, L., Panepucci, E., Wang, M., Shoeman, R. L., Schlichting, I. & Doak, R. B. (2015). *Acta Cryst.* D**71**, 387–397.
Boutet, S. *et al.* (2012). *Science*, **337**, 362–364.
Chapman, H. N., *et al.* (2011). *Nature (London)*, **470**, 73–77.
Coquelle, N., Brewster, A. S., Kapp, U., Shilova, A., Weinhausen, B., Burghammer, M. & Colletier, J.-P. (2015). *Acta Cryst.* D**71**, 1184–1196.
Deponte, D. P., Mckeown, J. T., Weierstall, U., Doak, R. B. & Spence, J. C. H. (2011). *Ultramicroscopy*, **111**, 824–827.
DePonte, D. P., Nass, K., Stellato, F., Liang, M. N. & Chapman, H. N. (2011). *Proc. SPIE*, **8078**, 8078OM.
Emma, P. *et al.* (2010). *Nat Photon.* **4**, 641–647.
Ishikawa, T. *et al.*, (2012). *Nat Photon.* **6**, 540–544.
Kern, J. *et al.* (2013). *Science*, **340**, 491–495.
Ko, I. S. *et al.* (2017). *Appl. Sci.* **7**, 479.
Liu, W., Ishchenko, A. & Cherezov, V. (2014). *Nat. Protoc.* **9**, 2123–2134.
McNeil, B. W. J. & Thompson, N. R. (2010). *Nat Photon.* **4**, 814–821.
Neutze, R., Wouts, R., van der Spoel, D., Weckert, E. & Hajdu, J. (2000). *Nature (London)*, **406**, 752–757.

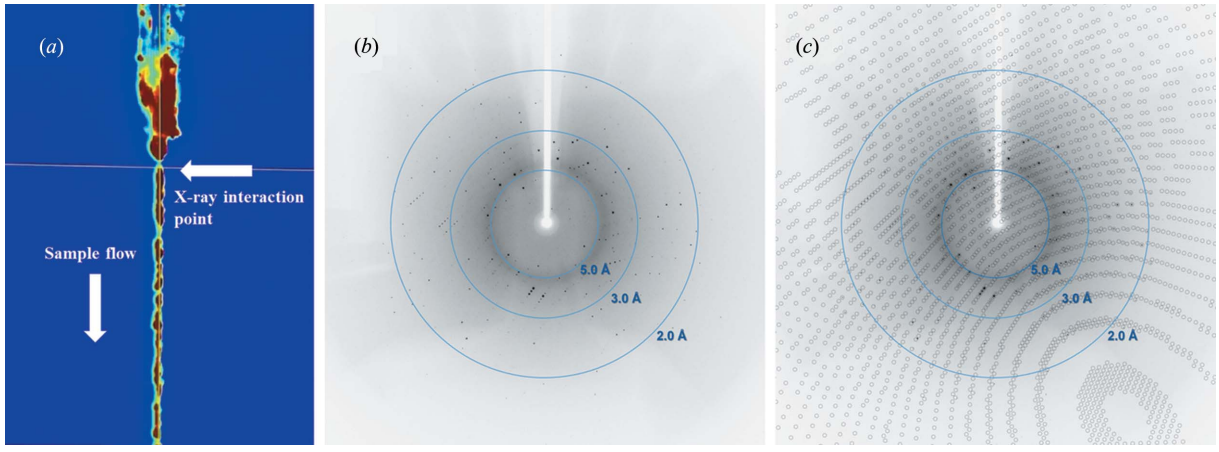

Figure 6
(*a*) Sample monitoring display during the CMD injector operation. (*b*) Single XFEL pulse diffraction pattern of the lysozyme crystal. (*c*) Indexing result of the diffraction pattern as obtained using *CrystFEL*.

Park, J., Kim, S., Nam, K. H., Kim, B. & Ko, I. S. (2016). *J. Kor. Phys. Soc.* **69**, 1089–1093.
Redecke, L. *et al.*, (2013). *Science*, **339**, 227–230.
Sierra, R. G. *et al.*, (2012). *Acta Cryst.* D**68**, 1584–1587.
Sugahara, M., Mizohata, E., Nango, E., Suzuki, M., Tanaka, T., Masuda, T., Tanaka, R., Shimamura, T., Tanaka, Y., Suno, C., Ihara, K., Pan, D., Kakinouchi, K., Sugiyama, S., Murata, M., Inoue, T., Tono, K., Song, C., Park, J., Kameshima, T., Hatsui, T., Joti, Y., Yabashi, M. & Iwata, S. (2015). *Nat. Methods*, **12**, 61–63.
Tono, K., *et al.* (2015). *J. Synchrotron Rad.* **22**, 532–537.
Weierstall, U., Doak, R. B., Spence, J. C. H., Starodub, D., Shapiro, D., Kennedy, P., Warner, J., Hembree, G. G., Fromme, P. & Chapman, H. N. (2008). *Exp. Fluids*, **44**, 675–689.
Weierstall, U., James, D. *et al.* (2014). *Nat. Commun.* **5**, 3309.
Weierstall, U., Spence, J. C. H. & Doak, R. B. (2012). *Rev. Sci. Instrum.* **83**, 035108.
White, T. A., Mariani, V., Brehm, W., Yefanov, O., Barty, A., Beyerlein, K. R., Chervinskii, F., Galli, L., Gati, C., Nakane, T., Tolstikova, A., Yamashita, K., Yoon, C. H., Diederichs, K. & Chapman, H. N. (2016). *J. Appl. Cryst.* **49**, 680–689.